Journal of Power Sources 195 (2010) 5206–5212

Contents lists available at ScienceDirect

Journal of Power Sources

journal homepage: www.elsevier.com/locate/jpowsour

Thermodynamic analysis of interactions between Ni-based solid oxide fuel cells (SOFC) anodes and trace species in a survey of coal syngas

Andrew Martinez[b,c], Kirk Gerdes[a,*], Randall Gemmen[a], James Poston[a]

[a] National Energy Technology Laboratory, U.S. Dept of Energy, 3610 Collins Ferry Road, Morgantown, WV 26507, USA
[b] Mickey Leland Energy Fellowship, U.S. Dept of Energy, National Energy Technology Laboratory, 2009, USA
[c] Dept. of Mechanical Engineering, Building 520, Stanford University, Stanford, CA 94305, USA

ARTICLE INFO

Article history:
Received 27 January 2010
Received in revised form 4 March 2010
Accepted 5 March 2010
Available online 20 March 2010

Keywords:
Solid oxide fuel cells
Gasification
Contaminants
Anodes
Thermodynamic analysis
Trace elements

ABSTRACT

A thermodynamic analysis was conducted to characterize the effects of trace contaminants in syngas derived from coal gasification on solid oxide fuel cell (SOFC) anode material. The effluents from 15 different gasification facilities were considered to assess the impact of fuel composition on anode susceptibility to contamination. For each syngas case, the study considers the magnitude of contaminant exposure resulting from operation of a warm gas cleanup unit at two different temperatures and operation of a nickel-based SOFC at three different temperatures. Contaminant elements arsenic (As), phosphorous (P), and antimony (Sb) are predicted to be present in warm gas cleanup effluent and will interact with the nickel (Ni) components of a SOFC anode. Phosphorous is the trace element found in the largest concentration of the three contaminants and is potentially the most detrimental. Poisoning was found to depend on the composition of the syngas as well as system operating conditions. Results for all trace elements tended to show invariance with cleanup operating temperature, but results were sensitive to syngas bulk composition. Synthesis gas with high steam content tended to resist poisoning.

Published by Elsevier B.V.

1. Introduction

By 2030, consumption of coal in the United States will increase by 19% over the 2006 level of 112 million short tons, with 92% of that coal being used for generating electricity [1,2]. To simultaneously accommodate expanded coal consumption and anticipated emission regulation, clean coal technology including integrated gasification fuel cell (IGFC) and integrated gasification combined cycle (IGCC) plants have been investigated [3–6]. Coal gasification technology has been proposed to achieve a higher conversion efficiency by combining coal and an oxidant (oxygen or air) at elevated temperature and pressure to produce synthesis gas (syngas), which is subsequently combusted and expanded in a turbine or fuel cell/turbine hybrid cycle. The syngas is generally comprised of H_2, H_2O, CO, CO_2, N_2, and CH_4, although the specific syngas composition depends on gasifier design, operating conditions, coal source, and other parameters. The coal syngas also contains trace amounts of volatile elements present in the solid coal.

Advanced power generation technologies that include solid oxide fuel cells (SOFCs) directly convert syngas chemical potential to electricity at high efficiency [7]. Typical SOFC anodes contain 40–60 wt% nickel, which imparts favorable microstructure, electrical conductivity, thermal robustness, and catalytic activity to the anode. However, trace materials contained in coal-derived syngas may negatively affect anode performance under typical fuel cell operating conditions. Thermodynamic studies that consider a single bulk syngas composition have demonstrated the effect of system operating conditions on the trace species present in coal syngas [8,9]. Experimental studies have shown trace species interactions with the anode nickel, typically for a single simulated syngas composition [8–14]. Published research examining the effect of bulk syngas composition on the partitioning of trace materials and interaction with the SOFC anode is not available.

The purpose of the current thermodynamic study is to examine the impact of bulk gas composition on the distribution of trace materials and secondary phases in a gasifier-cleanup-fuel cell process train. In particular, the raw coal syngas composition is related to the trace species interaction with the nickel-based SOFC anode. In this study, a thermodynamic simulation is developed that describes the elemental partitioning of syngas from generation in the gasifier, through warm gas cleanup, and to equilibration with a nickel-based SOFC. The study considers 15 syngas compositions, operation of the warm gas cleanup system at two temperatures, and operation of the SOFC at three different temperatures. Syngas input to the simulation is normalized on an electrochemical performance basis to permit a common evaluation of the results.

* Corresponding author. Tel.: +1 304 285 4342; fax: +1 304 285 0903.
E-mail address: kirk.gerdes@netl.doe.gov (K. Gerdes).

0378-7753/$ – see front matter. Published by Elsevier B.V.
doi:10.1016/j.jpowsour.2010.03.046

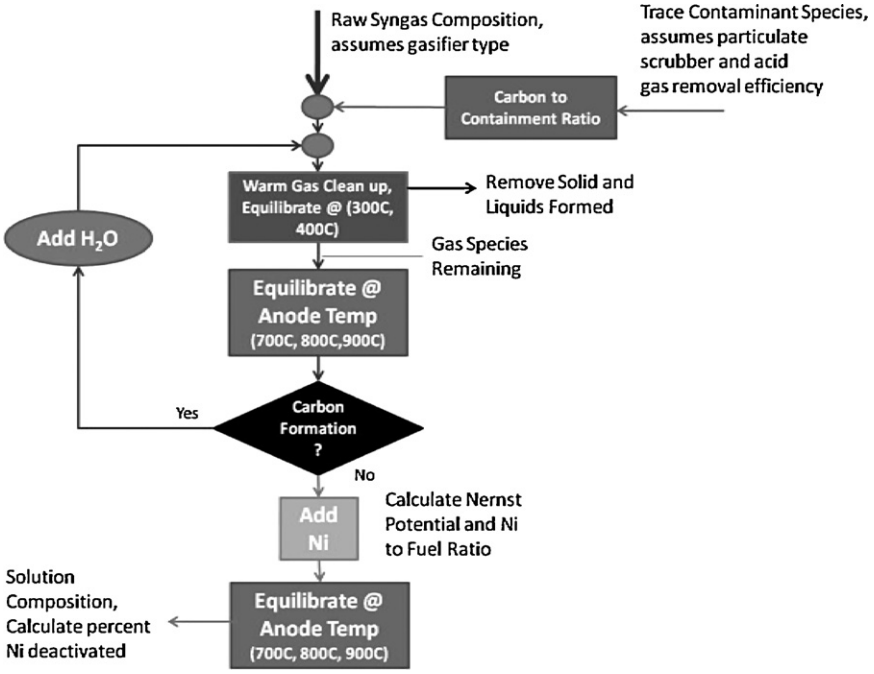

Fig. 1. Computational flow diagram for syngas/anode equilibrium calculation.

2. Methods

The thermodynamic modeling package FactSage v6.1 was implemented to calculate the thermodynamic equilibrium condition of each process stage. The equilibrium module of the FactSage software minimizes Gibbs free energy given a fully defined thermodynamic state (T,P,μ). The equilibrium calculations were performed within a larger program constructed using macros within the FactSage software package. The FactSage macro interfaced with an Excel workbook to reference input conditions, record output, and generate graphical results.

The equilibrium analysis was completed in two stages, a cleanup stage analysis (CSA) and an anode reaction analysis (ARA), mirroring the framework of Trembly et al. [9]. The CSA investigates the effects of operating temperature and pressure on trace species condensation within the warm gas cleanup system. The species that condense during CSA are considered removable by high temperature filtration and are therefore not passed through to the ARA stage. The ARA stage accepts the CSA gaseous effluent results and predicts the thermodynamic equilibrium species present given the operating condition of the inlet of a solid oxide fuel cell with a nickel anode.

The simulation includes 15 raw syngas compositions which are characteristic of 15 different gasifiers. The analysis considers two clean up temperatures and three different fuel cell (anode) operating temperatures. The parameter space spans all combinations of syngas composition, CSA temperature, and ARA temperature for a total of 90 separate cases.

Fig. 1 depicts the generally linear calculation path, and iteration is only necessary when water addition is required to mitigate carbon formation. The syngas produced from each gasifier first requires trace material addition, which simulates a common source of coal used for all gasifier cases. The program applies a carbon-to-trace-material correction factor which effectively adds trace species as necessary such that the ratio of carbon and contaminant in the syngas is normalized. Syngas containing trace material is then passed into the CSA routine where it is equilibrated at the cleanup stage conditions (T,P) and resulting condensates are removed. The syngas CSA composition is passed to the ARA stage and is first equilibrated at the anode temperature. The resulting composition is used to generate a Nernst correction factor that is applied to preserve the ratio of calculated fuel quality to anode nickel. The corrected mixture is equilibrated again at the anode temperature with the mass of nickel required by the Nernst factor. The product species from this final equilibration indicate the secondary phases formed on the anode, and the species that exit the fuel cell with no interaction.

2.1. Raw syngas composition

The simulation parameter space is defined relative to the operating domain of current and near-term gasification, cleanup, and SOFC technology. In total, 15 different gasifiers were investigated as part of this study, with raw syngas compositions shown in Table 1. The gasifiers are selected on the basis of the syngas composition generated to achieve the greatest possible variation. This facilitates the study's goal of generality regarding degradation of the SOFC anode upon syngas exposure, yet imposes technically achievable gas compositions.

The trace species assumed present in the coal syngas in this study were based on data collected from past measurements from various entrained flow gasification systems [9,15–18]. The contaminant profile described by Trembly et al. [9] is adopted. The concentrations and species listed in Table 2 assume that particulate filtering occurs upstream of the warm gas clean up stage to remove larger particles. The exact concentration of trace species used for each gasifier syngas case was normalized to maintain the same carbon to total contaminant ratio for each case.

Simplifying model assumptions were made to maintain a physically appropriate model while observing limitations of the FactSage software. First, solid carbon formation was suppressed during CSA by iteratively adding water. In order to make the results more conservative (increasing the impact on the fuel cell) it was assumed that carbon could only form on the anode and not in the cleanup process. Water was supplied upstream in the proportion required to negate carbon formation on the anode. Second, sodium and potassium were not included in the analysis in order to preserve phosphorous in the CSA. Retention of sodium and potassium in

Table 1
Raw coal syngas compositions for each gasifier.

Gasifier	H_2	CO	CO_2	N_2	H_2O	CH_4
Schwartz Pumpe	62.15%	26.31%	2.81%	1.81%	0.00%	6.93%
Exxon Singapore	44.59%	35.47%	17.94%	1.40%	0.10%	0.50%
Tampa	37.20%	46.60%	13.30%	2.50%	0.30%	0.10%
El Dorado	35.40%	45.00%	17.10%	2.10%	0.40%	0.00%
Fife	34.54%	55.62%	1.61%	3.11%	0.00%	5.12%
Pernis	34.40%	35.10%	30.00%	0.20%	0.00%	0.30%
KBR	34.50%	35.20%	30.09%	0.20%	0.00%	0.00%
Valero-Delaware	32.00%	49.50%	15.80%	2.20%	0.40%	0.10%
KRW	29.51%	51.83%	12.47%	0.91%	0.10%	5.17%
Eastman	31.12%	38.39%	13.13%	0.69%	16.67%	0.00%
PSI	24.78%	39.46%	9.29%	2.30%	22.68%	1.50%
Entrained*	29.30%	28.70%	11.80%	3.00%	27.20%	0.00%
Sarlux	22.70%	30.60%	5.60%	1.10%	39.80%	0.20%
ILVA	8.64%	26.33%	14.07%	42.71%	0.00%	8.24%
Catalytic gasifier	15.00%	5.00%	21.80%	1.00%	38.90%	17.50%

the CSA generates sodium/potassium phosphates, which would condense and be removed. Preserving the phosphorous content provides for a more aggressive estimate of total Ni consumed due to the trace contaminants, than in simulations which exclude phosphorus.

In the ARA module, formation of solid carbon (coke) is considered, since anodic carbon formation has been experimentally observed and is typically detrimental to the operation of the fuel cell. In practice coke formation is suppressed by the addition of steam to the fuel feed. Although the exact mechanism of carbon suppression is unknown, thermodynamic simulations indicate that the additional oxygen reacts with the carbon to form carbon dioxide.

The water addition step in the analysis is performed iteratively as indicated in Fig. 1. The program first checks for carbon formation and adds water to the raw syngas composition as necessary to completely suppress carbon formation. This iterative process is performed with the implementation of a Newton–Raphson technique to expedite the computational time. The amount of water added is the minimum amount to completely eliminate carbon formation.

2.2. Unit operations

The CSA was performed at temperatures of 315 °C and 400 °C with a pressure of 20 atm. These two warm gas clean up temperatures were investigated as reasonable operating points given the requirement to condense a majority of the trace contaminants while maintaining exergy [8,9]. The goal of the clean up stage is to remove traces species that are either environmentally toxic or could have an adverse effect on the system. The effectiveness of the warm gas cleanup stage is assumed to be 100%, and any formed condensate, whether liquid or solid, is removed completely. Although high temperature operation is advantageous from a system efficiency perspective, construction and operation of a robust SOFC is more difficult. The ARA considers SOFC operating temperatures at 700 °C, 800 °C and 900 °C. For all cases, the operating pressure was specified at 1.05 atm.

2.3. Normalization of model input

The analysis implements two correction factors to maintain congruence between the different syngas compositions and produce equitable comparisons between the fuel cells operated on the various syngas compositions. First, there is contaminant to carbon normalization that simulates a common coal source. Second, there is energy normalization based on the equilibrated syngas Nernst potential at the inlet of the SOFC.

Although there has been an ongoing effort to accurately catalogue the concentration of trace contaminants in coal-derived gas streams, the exact contaminant species and gas composition are dependent on the coal source and gasifier technology leading to some level of uncertainty in exact concentrations. To apply a common contaminant load for each fuel, a trace contaminant profile (Table 2) based on the Eastman Chemical Company's analysis from their coal complex in Kingsport, TN was applied across all raw syngas compositions. The trace species profile was scaled to the carbon content of the raw syngas, thereby raising the absolute contaminant content (by moles) of fuels that contain greater carbon relative to other fuel constituents. Since the carbon contained in raw syngas is directly related to the amount of coal used to create that syn-

Table 2
Beginning trace species concentrations for each gasifier.

Component	Concentration
AsH3	6.0E−07
HCl	1.0E−06
PH3	1.9E−06
Sb	7.0E−08
Cd	1.1E−08
Be	2.5E−08
Cr	6.0E−06
Hg	2.5E−08
K	0.0E+00
Se	1.5E−07
Na	0.0E+00
V	2.5E−08
Pb	2.6E−07
Zn	9.0E−06
H2S	1.0E−05
COS	1.0E−07

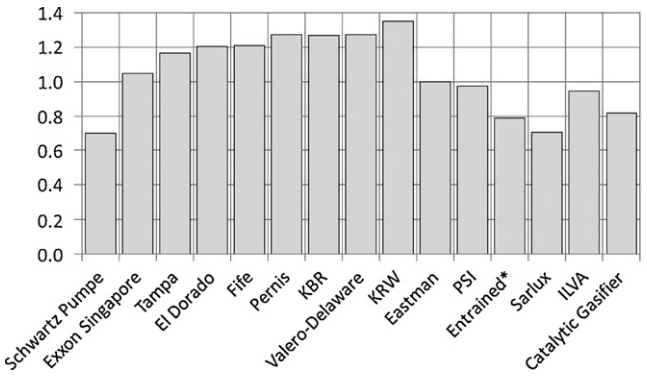

Fig. 2. Scaling factor required to maintain C:trace material ratio (standardized on Eastman).

Table 3
Fuel cell operating parameters.

Specified variables, fuel cell characteristics		
η_{cell}	Cell efficiency	80%
R_{ohmic}	Ohmic resistance	0.1 ohm cm^2
FU	Fuel utilization	80%
V_{act}	Activation loss	0.1 V
t	Time	1000 h
ρ_{Ni}	Anode Ni density	0.15 mol cm^{-3}
T_{cell}	Anode thickness	250 μm
V_{Nernst}	Nernst potential	0.92–1.12 V
n_{fuel}	Charge number (e^- mol_{fuel}^{-1})	0.77–2.02

gas [14], the contaminant content will scale directly. Fig. 2 depicts the contaminant scaling factor used to maintain the proper ratio of contaminants to the number of carbon atoms for each of the raw syngas compositions considered. The factors are normalized to the Eastman gasifier.

To maintain equality between each syngas composition on an energy basis, another correction factor is used to normalize the energy density of each fuel. The syngas is equilibrated at the inlet of the fuel cell, and the resulting composition is used to calculate the Nernst potential and the charge number. Nernst potential and charge number are calculated by averaging the values obtained from individual reactions of hydrogen, carbon monoxide, and methane. The calculated Nernst potential and physical parameters from a model fuel cell were used to relate the number of moles of syngas to the number of moles of nickel using the equation:

$$\frac{N_{Ni}}{N_{fuel}} = \frac{FU \times T_{cell} \times n_{fuel} \times F \times R_{ohmic} \times \hat{\rho}_{Ni}}{[V_{Nernst} \times (1 - \eta_{cell}) - V_{act}] \times t}. \quad (1)$$

Here, N is the number of moles [mol], FU is the fuel utilization factor [%], T is the temperature [K], n is the number of electrons per mole of fuel reacted [e^- mol^{-1}], F is Faraday's constant [C mol^{-1}], R is the ohmic resistance [ohm cm^2], ρ_{Ni} is the molar density of the nickel anode [mol cm^{-3}], V_{Nernst} is the Nernst potential [volts], η is the fuel cell stack efficiency [%], V_{act} is the activation overpotential [volts], and t is the time of operation [h]. The derivation of Eq. (1) is shown in Appendix A. Typical values for each of the parameters are shown in Table 3, and nickel to syngas ratios for each syngas composition are depicted in Fig. 3.

This ratio normalizes the fuel to nickel ratio on the basis of common energy output, and each starting syngas composition requires a unique corrective Nernst factor. For example, syngas with lower energy density requires more fuel to achieve the target power output and therefore the syngas to nickel ratio would be larger. As shown in Eq. (1) and Appendix A, the anode irreversible losses are attributed to ohmic resistance (η) and activation polarization. The thermodynamic model does not include effects of diffusion polarization as a function of temperature, given that the effect is

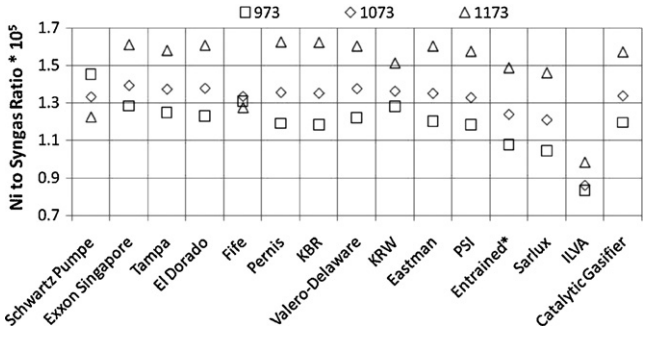

Fig. 3. Ni to syngas ratio as a function of fuel cell operating temperature with CSA temperature of 588 K.

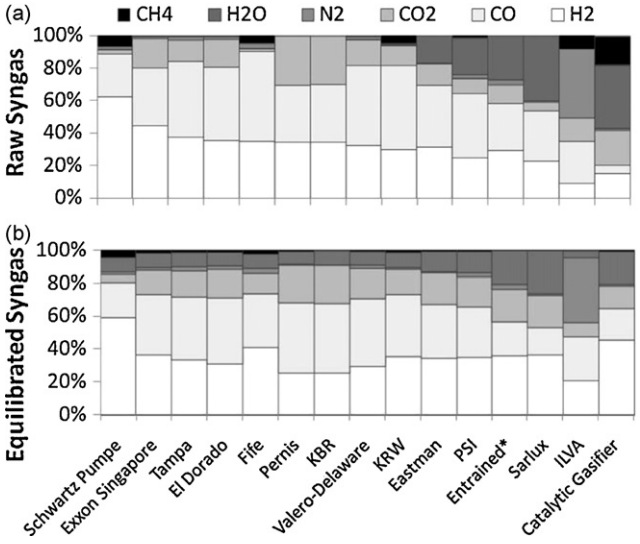

Fig. 4. (a) Raw syngas composition (bulk gas); (b) equilibrated syngas at 973 K.

expected to be small over the ranges of temperature and current density investigated.

3. Results and discussion

The thermodynamic analysis is performed as described above and results are described in order of procession through the simulation. The final nickel to syngas ratio determined after normalization of the fuels is depicted in Fig. 3 for each gasifier. Syngas composition (quality) affects the quantity of fuel required to produce a standard amount of energy, and those gas compositions containing proportionally fewer fuel molecules (H_2, CO, CH_4) require the greatest amount of total fuel relative to the anode nickel content. Most fuel composition to nickel ratios has a directly proportional relationship with temperature. In general, the lower the temperature the higher the Nernst potential and the less fuel required to produce the same amount of energy. However, there are several outlying cases, most predominately the Schwartz Pumpe and Fife cases, which do not follow this trend. Those exceptions are cases that require water addition, which suppresses carbon formation and also depresses the Nernst potential and charge number of the syngas. As temperature increases in the outlying cases, suppression of carbon formation requires addition of less relative water, and fuel dilution by water addition is less severe.

3.1. Syngas composition

Graphical representations of the bulk and equilibrated syngas compositions are given in Fig. 4. Fig. 4(b) depicts equilibrated syngas composition at an anode temperature of 700 °C (973 K). At the elevated temperatures of 800 °C and 900 °C the concentrations of H_2 and CO increase while the CH_4 and H_2O concentrations typically decrease. The simulation permits instantaneous heat transfer to equilibrate the gas mixture at the fuel cell operating temperature. In practice, a small pre-equilibration section may be required for heat transfer purposes, but the shift and reforming reactions are known to occur relatively quickly and therefore support the equilibrium assumption.

Although most pre- and post-equilibration compositions are similar, some differences exist that reflect non-equilibrium conditions of the initial gas composition. In particular, the ILVA and catalytic gasifier demonstrate substantial shifts, indicating an initially large non-equilibrium. In practice, substantial changes

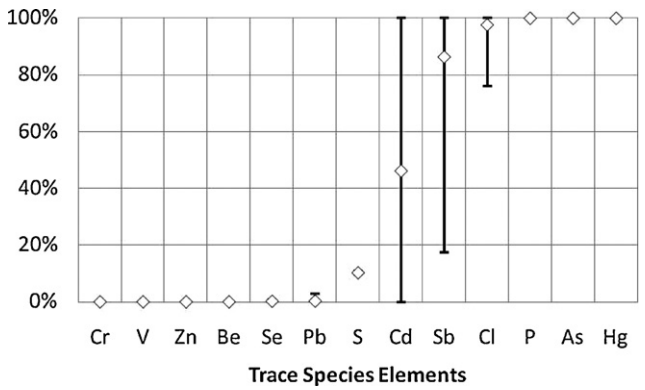

Fig. 5. Percentage of entering trace species that pass through CSA for all cases and all temperatures. Error bars represent the range of each element that is thermodynamically predicted in all scenarios.

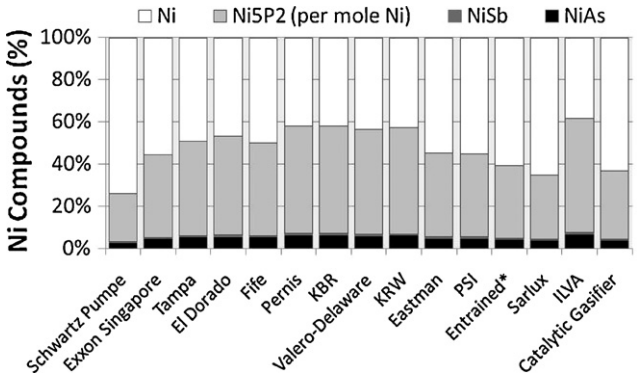

Fig. 6. Ni species distribution in anode after 3000 h with ARA temperature of 973 K and CSA temperature of 673 K.

in equilibrium composition will consume or release substantial energy, which may impact the operating temperature of the system and cause undesirable impacts on the thermal profile. In the case of the ILVA and catalytic gasifier, the CH_4 will preferentially shift into CO_2 and H_2 in an endothermic reaction, which requires energy transfer to the system. If the energy for the reforming reaction is not supplied properly in practice, the temperature of the fuel cell could be sharply impacted.

3.2. Cleanup stage analysis

As discussed earlier, sodium and potassium were removed from the trace species list (Table 2) so that sodium phosphates and/or potassium phosphates cannot precipitate, thereby removing the phosphorus load. This assumption is validated by operational observations of sodium and potassium removal in gasifier slag [19], and by recognizing the severe impact that phosphorus has on cell performance. Fig. 5 shows that warm gas cleanup eliminates Cr, V, Zn, Be, and Se with 100% efficiency, indicating that the species partition entirely to liquid or solid phases. Other species such as Pb, S, Cd, Sb and Cl, are partitioned between gas and liquid/solid phases according to the operating conditions of the CSA and ARA. Three species, Hg, As, and P, are not condensed and fully pass through the CSA at all conditions in the investigated range.

The primary species demonstrating a propensity to form secondary phases with the anodic nickel are arsenic (As), phosphorus (P), and antimony (Sb). As indicated in Fig. 5, arsenic and phosphorous readily pass through the CSA at all operating conditions. Sb phase partitioning depends on the CSA temperature and syngas composition. Results for those gasifier compositions that require water (ILVA, Fife, El Dorado, Valero-Delaware, Tampa, and KRW) all show that at lower anode temperatures, the additional hydrogen and oxygen preferentially shift Sb(s) to SbO_2H_2(g). As and P are present in higher concentrations than Sb so the presence of these species in the SOFC causes more secondary phase formation. Although warm gas cleanup does affect the Sb concentration, the amount of Sb present initially is such a small concentration that the exergy loss associated with operating the clean up stage at a lower temperature is expected to be more detrimental than the SOFC deactivation observed from the Sb poisoning.

3.3. Anode reaction analysis

By exploring an aggressive contaminant interaction scenario, the contaminant species forming secondary nickel phases most readily are identified for the range of operating conditions considered. Fig. 6 depicts the relative partitioning of the anode nickel between the primary Ni-containing phases for a simulated operating time of 3000 h with CSA temperature of 400 °C (673 K) and an ARA temperature of 700 °C (973 K). Under the experimental conditions utilized in these simulations, the SOFC would be deactivated primarily by the trace contaminants As and P, with Sb playing a minor role. The relative impact of each trace material parallels the source gas contaminant load. The simulations conducted at different ARA temperature conditions indicates that arsenic poisoning is sensitive to the operating temperature of the fuel cell only whereas phosphorous and antimony poisoning are sensitive to both syngas composition and operating conditions. The temperature parameters used to generate Fig. 6 produce the most aggressive contaminant-loading scenario, with all As, P, and Sb passing through cleanup and forming nickel compounds.

The impact of the trace materials is estimated using a model SOFC anode consisting of pure, dense nickel. In practice, the SOFC anode is formed from a porous cermet matrix, generally incorporating yttrium stabilized zirconium (YSZ). Studies have shown that the thermodynamics and kinetics governing the reactivity of pure metals differ from those of a similar metal incorporated into a ceramic matrix, with a general suppression of metal reactivity to specific gas for the cermet material [20–23]. Further, the absolute values assigned to anode thickness and nickel density are adjustable as long as the total nickel mass is conserved. For example, a 250 μm dense nickel electrode contains the same mass as a 500 μm, 50% porous electrode. Although the present study does not simulate an exact SOFC anode fuel gas interaction, it does capture the scales pertaining to relative deactivation for the cases studied and strongly indicates that of all the trace contaminants found in coal-derived fuel gas, As, P and Sb pose the greatest potential for anodic attack.

3.3.1. Arsenic (As)

As seen in Fig. 7(a), nickel–arsenic compounds are present only at 973 K and 1073 K, and formation of the secondary phase is relatively independent of gasifier composition. Compositional insensitivity is explained by noticing that the primary As specie remaining after CSA is primarily As_4(g), with only a minor amount of As–H gaseous forms present. Therefore the equilibrium species of As are primarily weakly coupled compounds (small amount of equilibrium AsH_4) and are insensitive to the bulk syngas composition.

Within the FactSage databases, reliable Ni–As thermodynamic properties exist for NiAs and $Ni_{11}As_8$, which include heat capacity properties; however, insufficient data exist for common experimentally observed species of Ni–As such as Ni_5As_2, Ni_3As_2, and $NiAs_2$ [24,25]. Although Ni_5As_2 and $Ni_{11}As_8$ are not formed using the existing FactSage databases, the databases are unaltered to maintain congruence with other FactSage users. Adjustment of the

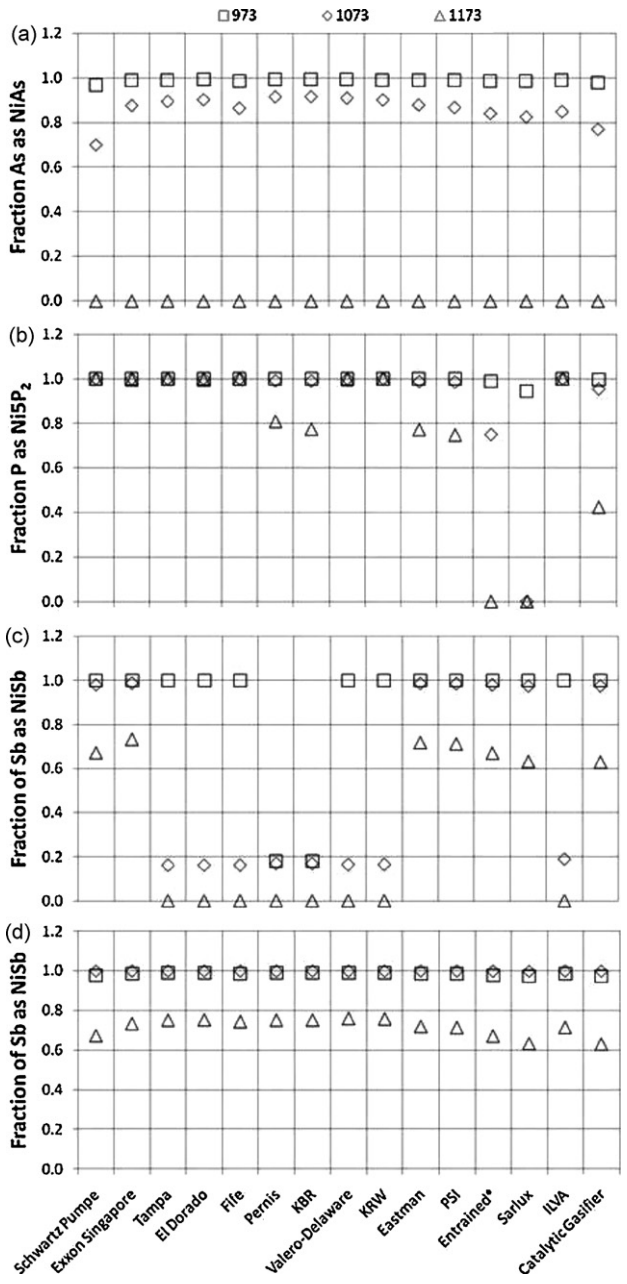

Fig. 7. (a) Arsenic present as NiAs (result is independent of CSA temperature); (b) phosphorus present as $Ni5P_2$ (result is independent of CSA temperature); (c) antimony as NiSb at CSA temperature of 588 K; (d) antimony as NiSb at CSA temperature of 673 K.

databases to include additional nickel–arsine phases may be performed in a future effort.

3.3.2. Phosphorous (P)

Anodic nickel–phosphorous compounds are formed at nearly every operating condition examined in this investigation, as indicated in Fig. 7(b). Phosphorous poisoning is particularly interesting because of the predicted sensitivity to syngas composition. In most cases, the phosphorous completely forms secondary phases with nickel, with no residual phosphorus species exiting the fuel cell system. However, predictions for the entrained and Sarlux gasifiers indicates little Ni–P phase formation, even at the intermediate temperature of 1073 K. Cross comparing the equilibrium composition shown in Fig. 4(b), it is noted that these two gasifiers produce a syngas that is relatively rich in steam. The additional oxygen generates phosphorous trioxides $(P_2O_3)_{2(g)}$, at the higher ARA temperatures. $(P_2O_3)_{2(g)}$ forms preferentially over the Ni–P phases, thereby removing the phosphorus from participation in a reaction with anodic nickel. A similar but diminished effect is apparent in other cases that include substantial water, such as the catalytic gasifier.

The FactSage databases included in the analysis predict that the only Ni–P compound generated is Ni_5P_2. Although this result is consistent with some experimental data, controversy remains regarding the exact values of some thermodynamic parameters included in the databases [26–29], and the tendency of the phosphorus to form Ni_3P or Ni_5P_2. The exact values assigned to thermodynamic data (whether using original FactSage databases or using slightly modified databases) will modestly alter the results, because a different phase will effectively change the Ni consumption rate (from 3:1 for Ni_3P formation to 2.5:1 for Ni_5P_2). The present analysis retains the unaltered FactSage thermodynamic data to preserve congruence with other FactSage users. The discrepancy in thermodynamic data requires resolution; however, retaining the packaged thermo-data is judged most prudent for the present analysis. More formal investigation into the preferred phase formation and resolution of the accompanying thermodynamic data should be completed before the present datasets are updated.

3.3.3. Antimony (Sb)

Fig. 7(c) and (d) depict the extent of secondary anodic phase formation for CSA temperatures of 315 °C and 400 °C, respectively. Comparison of the two figures indicates the relative impact of the CSA temperature, which uniquely impacts Sb by permitting substantial pre-SOFC removal in the cleanup system. When present, antimony readily reacts with the anode nickel, and demonstrates an indifference to bulk syngas composition. Although Sb can be removed at a lower cleanup temperature, it may be disadvantageous from a system perspective, as the lower the cleanup temperature will destroy exergy and diminish the overall system efficiency. Further, antimony is only present in small amounts and therefore does not affect the cell performance as drastically as As and P.

3.4. Chemical kinetics and thermodynamic equilibrium assumption

It must be explicitly stated that the fundamental assumption of thermodynamic equilibrium underlies the entire analysis. Some chemical kinetics and reaction rates are known for the various reactions, but the sheer complexity of chemistry prevents direct experimentation in many instances. Difficulty is compounded given the trace concentrations of the participating species. Assumption of bulk syngas equilibrium at the inlet of the SOFC is reasonable because the primary syngas reactions (water gas shift and steam reforming of methane) are known to occur quickly. However, similar logic is not applicable to the trace species. In practice, species transport limitations or slow chemical kinetics may prevent nickel reaction at the level described here. Further, the electrochemical processes may reverse some unwanted reactions and mitigate deactivation. The thermodynamic data are well characterized with the exceptions already discussed. The analysis may therefore be regarded as an upper limit on trace material interaction within the fuel cell.

4. Conclusion

In the present work, the effect on fuel cell performance of trace contaminant species found in coal syngas from 15 different gasifiers was investigated. Arsenic, phosphorous, and antimony form

unwanted anodic nickel compounds, but the magnitude of reaction was dependent on unique thermodynamic parameters for each of the systems considered. Generation of arsenic compounds is most sensitive to the temperature of fuel cell operation, with no Ni–As phases produced at SOFC operating temperatures above 900 °C. Phosphorus was sensitive to the bulk gas composition, with suppression of the Ni–P phases by addition of steam. Antimony compounds were sensitive to the temperature of warm gas cleanup, with fewer Ni–Sb phases produced when operating the gas cleanup system at 315 °C. Results indicate that strategies to diminish the impact of trace materials on the SOFC include adding active nickel capture beds operating below 700 °C, adding steam, and operating the SOFC at elevated temperatures.

Appendix A. Derivation of Eq. (1)

Eq. (1) is generated to relate the syngas to nickel ratio as a function of standard cell parameters and gas composition. Although gas composition varies between gasifiers, for fair comparison, it is necessary to ensure that the simulated fuel cells have equivalent power output in all systems. Power output of the fuel cell is defined by

$$P = A_{cell} \times i'' \times V_{cell} \times N_{cells}. \tag{A1}$$

The total current permitted across the cell can be related to the number of reactions occurring on the cell according the equation

$$N_{cell} \times A_{cell} \times i'' = FU \times \frac{N_{fuel} \times n_{fuel} \times F}{t}. \tag{A2}$$

The observed cell voltage can be related to the Nernst potential through either the cell efficiency or the component polarization losses as

$$V_{cell} = V_{Nernst} \times \eta_{cell} = V_{Nernst} - V_{act} - i'' R_{ohm}. \tag{A3}$$

Finally, the moles of nickel that are used in the cell can be determined from the density and electrode geometry as

$$N_{Ni} = A_{cell} \times T_{cell} \times \hat{\rho}_{Ni} \times N_{cell}. \tag{A4}$$

Eqs. (A1) through (A4) may be combined to obtain the nickel to syngas ratio (N_{Ni}:N_{fuel}) required to maintain a constant output power. First, Eqs. (A1) and (A2) may be combined as to describe the moles of fuel required to generate a total power output given the cell operating parameters

$$N_{fuel} = \frac{P \times t}{FU \times F \times n_{fuel} \times V_{cell}}. \tag{A5}$$

Next, Eqs. (A1) and (A4) may be combined describe the number of moles of nickel required to operate the cell at a constant power output for the given cell operating parameters

$$N_{Ni} = \frac{P \times T_{cell} \times \hat{\rho}_{Ni}}{i'' V_{cell}}. \tag{A6}$$

Combining (A5) and (A6) to generate a ratio, and substituting Eq. (A3) for V_{cell} permits generation of Eq. (1)

$$\frac{N_{Ni}}{N_{fuel}} = \frac{FU \times T_{cell} \times n_{fuel} \times F \times R_{ohmic} \times \hat{\rho}Ni}{[V_{Nernst} \times (1 - \eta_{cell}) - V_{act}] \times t}. \tag{1}$$

References

[1] Energy Information Administration, International Energy Annual 2006, Energy Information Administration, 2006.
[2] Energy Information Administration, Annual Energy Outlook 2009 with Projections to 2030, DOE/EIA-0383, Energy Information Administration, 2009.
[3] H.C. Frey, E.S. Rubin, Environmental Science Technology 26 (1992) 1982–1990.
[4] A.K. Anand, C.S. Cook, J.C. Corman, A.R. Smith, Journal of Engineering for Gas Turbines and Power - Transactions of the ASME, 118 (4) (1996) 732.
[5] F. Calise, M. Dentice d'Accadia, A. Palombo, L. Vanoli, Energy 31 (2006) 3278–3299.
[6] Y. Haseli, I. Dincer, G.F. Naterer, International Journal of Hydrogen Energy 33 (2008) 5811–5822.
[7] Ryan O'Hayre, Suk-Won Cha, Whitney Colella, Fritz B. Prinz, Fuel Cell Fundamentals, 2nd ed., John Wiley & Sons, New York, United States of America, 2009.
[8] M. Diaz-Somoano, M.R. Martinez-Tarazona, Fuel 82 (2002) 137–145.
[9] J.P. Trembly, R.S. Gemmen, D.J. Bayless, Journal of Power Sources 163 (2) (2007) 986–996.
[10] A.L. Marquez, T.R. Ohm, J.P. Trembly, D.C. Ingram, D.J. Bayless, Journal of Power Sources 164 (2) (2007) 659–667.
[11] J.P. Trembly, R.S. Gemmen, D.J. Bayless, Journal of Power Sources 169 (2007) 347–354.
[12] J.P. Trembly, R.S. Gemmen, D.J. Bayless, Journal of Power Sources 171 (2007) 818–825.
[13] M Gong, X. Liu, J.P. Trembly, C. Johnson, Journal of Power Sources 168 (2) (2007) 285–298.
[14] F.N. Cayan, M. Zhi, S.R. Pakalapati, I. Celik, N. Wu, R. Gemmen, Journal of Power Sources 185 (2) (2008) 595–602.
[15] A.W. Wang, Task 3.5: Poison Resistant Catalyst Development and Testing, Design and Construction of the Alternative Fuels Field Test Unit and Liquid Phase Methanol Feedstock and Catalyst Life Testing at Eastman Chemical Company: Topical Report, 1997.
[16] A.E. Pigeaud, J.J. Helble, Coal Fired Power Systems 1994 – Advances in IGCC, June 21–23, 1994.
[17] A.E. Pigeaud, J.J. Helble, Trace Species Emissions for IGFC, Coal-Fired Power Systems 94 – Advances in IGCC, June 21–23, 1994.
[18] Air Products and Chemicals Inc., Removal of Trace Contaminants from Coal-Derived Synthesis Gas, Topical Report, March 2003.
[19] J. Ratafia-Brown, L. Manfredo, J. Hoffman, M. Ramezan, Major environmental aspects of gasification-based power generation technologies, Final Report to U.S. Dept of Energy, National Energy Technology Laboratory, December 2002.
[20] G.Q. Lu, J.C. Diniz da Costa, M. Duke, S. Giessler, R. Socolow, R.H. Williams, T. Kreutz, Journal of Colloid and Interface Science 314 (2) (2007) 589–603.
[21] U. Balachandran, T.H. Lee, L. Chen, S.J. Song, J.J. Picciolo, S.E. Dorris, Fuel 85 (2) (2006) 150–155.
[22] U. Balachandran, B. Ma, P.S. Maiya, R.L. Mieville, J.T. Dusek, J.J. Picciolo, J. Guan, S.E. Dorris, M. Liu, Solid State Ionics 108 (1–4) (1998) 363–370.
[23] R.V. Siriwardane, J.A. Poston, E.P. Fisher, Applied Surface Science 243 (1–4) (2005) 40–54.
[24] H. Gamsjager, J. Bugajski, T. Gajda, R.J. Lemire, W. Preis, Chemical Thermodynamics of Nickel, Elsevier, New York, 2005.
[25] C.A. Coyle, O.A. Marina, E.C. Thomsen, D.J. Edwards, C.D. Cramer, G.W. Coffey, L.R. Pederson, Journal of Power Sources 193 (2) (2009) 730–738.
[26] M.E. Schlesinger, Chemical Review 102 (11) (2002) 4267–4301.
[27] C. Xu, J.W. Zondlo, H.O. Finklea, O. Demircan, M. Gong, X.B. Liu, Journal of Power Sources, 193 (2) (2009) 739–746.
[28] O. Demircan, C. Xu, J. Zondlo, H.O. Finklea, Journal of Power Sources 194 (1) (2009) 214–219.
[29] G. Heinz, Chemical Thermodynamics of Nickel, 6th ed., Elsevier, NY, US, 2005.